PERSPECTIVE

Check for updates

Gaseous CO_2 electrolysis: latest advances in electrode and electrolyzer technologies toward abating CO_2 emissions

Kazuhide Kamiya, [ID] *[ab] Sora Nakasone,[a] Ryo Kurihara,[a] Asato Inoue,[a] Hazuki Irie,[a] Shoko Nakahata,[a] Yuta Nishina, [ID] [c] Satoshi Taniguchi,[d] Thuy T. H. Nguyen [ID] [de] and Sho Kataoka [ID] *[de]

The conversion of CO_2 into multicarbon (C_{2+}) products *via* electrochemical reduction is considered a key technology for the sustainable production of fuels and chemicals. The performance of high-rate gaseous CO_2 electrolysis is governed by interrelated factors such as the electrocatalysts, electrodes, electrolytes, and cell architectures. Despite the intensive focus on catalyst research, systematic studies addressing the other components remain scarce, leaving critical gaps in our understanding toward achieving higher performance in CO_2 electrolysis systems. The nanoscale design of catalyst surface electronic structures and the macroscale design of electrodes and electrolyzer architectures both influence the overall activity of the electrochemical system. In designing macroscale components, it is necessary to establish benchmarks based on a comprehensive evaluation of CO_2 emissions for the entire electrolysis process, because these parameters are directly linked to output metrics such as current density and cell voltage under practical operating conditions. This review summarizes recent advances in electrodes and electrolyzers, and through life-cycle assessment (LCA), evaluates key performance indicators (KPIs) for achieving negative emissions and assesses the current technology readiness of CO_2 electrolysis.

1 Introduction

Global anthropogenic CO_2 emissions reached a staggering 37.8 Gt per year in 2024, nearly 80 times greater than those from volcanic and tectonic activities.[1] The development of technologies that utilize CO_2 as an alternative carbon feedstock and convert it into valuable chemicals is therefore important.[2,3] A wide range of methodologies for effective CO_2 reduction, including biological,[4] thermochemical,[5] photochemical,[6] and electrochemical approaches,[2,3,7] have been extensively studied. Among them, electrochemical CO_2 reduction has attracted significant attention because a high CO_2 conversion rate is expected even at ambient temperature and pressure. However, the practical application of CO_2 reduction requires improvements in operating efficiency, product selectivity, and production rate.

To enhance the production rate (expressed as current density), the use of gas diffusion electrodes (GDEs), which enable CO_2 reduction to occur at the interface between the solid catalyst, liquid electrolyte, and gaseous CO_2, is a promising approach.[8,9] GDEs accelerate the reaction by mitigating mass transport limitations imposed by the inherently low diffusion coefficient and solubility of CO_2 in water. Because CO_2 reduction occurs at a complex three-phase boundary, the selectivity and reaction rate of the CO_2 reduction reaction (CO_2RR) are governed by various factors, including the electrocatalyst, electrode structure, and the electrolyzer configuration.

Among these factors, the electrocatalyst is a core component in the CO_2RR because it directly converts CO_2 molecules on its surface and thereby directly influences product selectivity. Electrodes composed of a noble metal such as Au or Ag preferentially produce carbon monoxide (CO), whereas those composed of a p-block metal such as Hg or Pb favor the formation of formic acid. In the 1980s, Hori *et al.* reported that using Cu plates or Cu single crystals as electrodes for the CO_2RR enables the efficient formation of C_1 to C_3 organic compounds, including methane, ethylene (C_2H_4), ethanol, and *n*-propanol.[10–13] More than 40 years after this discovery, Cu

[a]Research Center for Solar Energy Chemistry, Graduate School of Engineering Science, The University of Osaka, 1-3 Machikaneyama, Toyonaka, Osaka 560-8531, Japan. E-mail: kamiya.kazuhide.es@osaka-u.ac.jp

[b]Innovative Catalysis Science Division, Institute for Open and Transdisciplinary Research Initiatives (ICS-OTRI), The University of Osaka, 1-1 Yamadaoka, Suita, Osaka 565-0871, Japan

[c]Research Institute for Interdisciplinary Science, Okayama University, 3-1-1 Tsushimanaka, Kita-ku, Okayama, Japan

[d]Research Institute for Chemical Process Technology, National Institute of Advanced Industrial Science and Technology (AIST), Central 5, 1-1-1 Higashi, Tsukuba 305-8565, Ibaraki, Japan. E-mail: s-kataoka@aist.go.jp

[e]Integrated Research Center for CCUS Implementation, National Institute of Advanced Industrial Science and Technology (AIST), Central 5, 1-1-1 Higashi, Tsukuba 305-8565, Ibaraki, Japan

remains the only metallic element known to reproducibly and efficiently catalyze the formation of C_{2+} with practical selectivity at a good rate. However, because catalytic aspects of CO_2 electroreduction have been extensively studied over the years and are well summarized in numerous review articles,[14–16] a detailed discussion of the underlying technologies is beyond the scope of this paper.

Recent studies have increasingly demonstrated that gaseous CO_2RR performance is not solely determined by the catalyst but is also strongly affected by factors such as the electrode architecture, electrolyte composition, and overall electrolyzer design. In fact, compared with catalyst-focused studies, research papers addressing electrolyzer and system-level aspects are increasingly common, as evidenced by publication statistics.[17] Nevertheless, in contrast to the extensive research on electrocatalysts, comprehensive review articles focused on these other system components remain limited. In addition, discussions that relate key performance indicators (KPIs) for achieving negative emissions to the technological maturity of CO_2RR systems from the perspective of life-cycle assessment (LCA) are still insufficient and require further exploration.

When developing components such as electrodes and electrolyzers, researchers should consider multiple performance indicators comprehensively, including cell voltage, current density, and product selectivity. More importantly, these performance indicators are closely and intricately associated with the product yield and the electricity consumption during actual operation, directly influencing the overall greenhouse gas (GHG) emissions. That is, researchers must develop these components with clearly defined benchmarks to contribute meaningfully to the goal of negative emissions. Sahu *et al.* highlighted the importance of LCA in the CO_2RR systems. Their perspective primarily concentrated on CO_2 emissions associated with electrolyzer productions particularly regarding the use of critical minerals (*e.g.*, precious metals and rare earth elements).[18] In recent years, the application of prospective LCA, also known as ex-ante LCA, has played a crucial role in emerging technologies aimed at reducing CO_2 emissions. LCA enables a holistic analysis of the influence of multiple factors, including the utilization of renewable energy, the procurement of raw materials, and the selection of construction materials for electrolyzers, on overall CO_2 emissions across the full life cycle. For example, Yamaguchi *et al.* performed the prospective LCA using literature values for the CO_2RR system and evaluated the CO_2 emissions under hypothetical conditions.[19] They also identified the key performance indices and set their benchmarks. It is essential to systematically examine these benchmarks in light of current technological issues and advances. In addition, a clear understanding of these benchmarks should be strategically leveraged to promote the development of elemental technologies. Accordingly, this review provides a first integrated framework that links electrode/electrolyzer design with LCA. Beyond summarizing recent technological advances, we quantify how KPI improvements affect system-level CO_2e impacts. We then quantify the KPI levels required for net-negative operation and conclude with an appraisal of the current technology readiness of CO_2 electrolysis.

2 Electrode and electrolyzer technologies

2.1 Gas diffusion electrodes

In traditional CO_2 electrolysis, an immersed electrode setup has generally been used. In this configuration, CO_2 gas is bubbled into a liquid electrolyte and the dissolved CO_2 is supplied to an electrode completely immersed in the solution. The reaction proceeds at the solid–liquid interface between the catalyst and the electrolyte; consequently, the current density is limited by the solubility and mass transport of CO_2 in the solution. Therefore, the current density is typically limited to several tens of milliamperes per square centimeter. To overcome these limitations, researchers have recently used GDEs. These electrodes allow CO_2 gas to be directly supplied to the reaction interface in its gaseous state (Fig. 1). The cathodic reaction proceeds at a three-phase interface comprising the catalyst, the electrolyte, and gaseous CO_2, similar to the interface in H_2–O_2 fuel cells. However, both the structure and reactivity of the three-phase interface differ substantially between the two systems (Fig. 1).

In the cathode of fuel cells for the oxygen reduction reactions (ORR), carbon nanoparticles loaded with Pt (Pt/C) are commonly used as catalysts. The Pt/C-based catalyst layer is highly hydrophobic, suppressing electrolyte flooding and forming a thick gas/electrolyte mixture layer with a thickness on the order of tens of micrometers. As a result, the current densities can reach approximately 1–2 A cm^{-2}. Even if the catalyst layer is flooded in the electrolyte, the ORR simply stops because of the cessation of the O_2 supply; the faradaic efficiency (FE) remains unaffected because no other reaction occurs at the operating potential of the ORR (approximately 0.6 V *vs.* reversible hydrogen electrode (RHE)). By contrast, the electrocatalysts for CO_2 electrolysis are composed of hydrophilic materials such as metal nanoparticles, metal oxides, or metal–nitrogen-doped
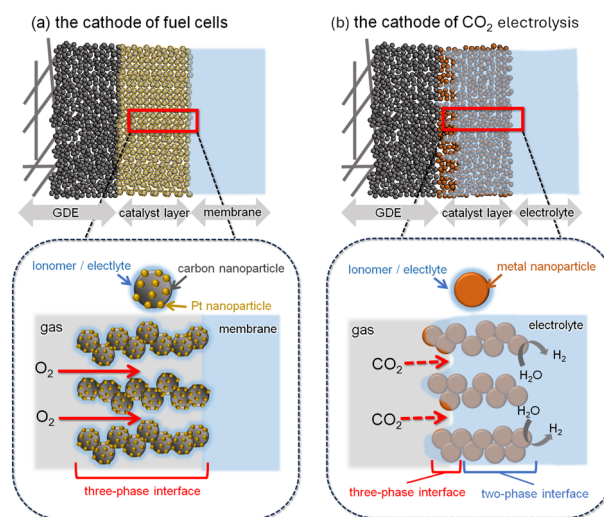

Fig. 1 Schematic of the reaction interfaces at (a) the Pt/C cathode in a fuel cell and (b) the metal-nanoparticle cathode in the gaseous CO_2RR.

carbons. Because of the hydrophilicity of electrocatalysts, the catalyst layer is easily flooded, substantially thinning the gas/electrolyte mixture layer.[20] In addition, the operating potential of CO_2 electrolysis is ~1.5 V lower than that of the cathode in fuel cells. Once the catalyst layer is submerged, the hydrogen evolution reaction (HER), a competing reaction, occurs, reducing the FE for the CO_2RR. Therefore, the three-phase interface in CO_2 electrolysis fundamentally differs from that in fuel cells and requires distinct design strategies. To achieve a high current density and product selectivity, expanding the effective three-phase interface area while minimizing the flooded regions is critical.

To address this challenge, Sargent *et al.* developed a hybrid catalyst by sputtering Cu onto a porous polytetrafluoroethylene (PTFE) sheet and subsequently loading it with Cu nanoparticles and a perfluorosulfonic acid ionomer.[21] This design achieved a partial current density of 1300 mA cm^{-2} for C_{2+} products formation in 7 M KOH.[21] In this architecture, gaseous reactants are efficiently transported through the hydrophobic domains of the ionomer, whereas ions are conducted through its hydrophilic domains and electrons through the Cu catalysts. The three-dimensional integration of Cu nanoparticles and an ionomer substantially enhances the diffusion of gaseous CO_2. As a result, the effective expansion of the three-phase boundary enables remarkably high current densities for C_{2+} products synthesis.

Xing *et al.* successfully doubled the partial current density for C_{2+} products formation by incorporating PTFE nanoparticles into a catalyst layer composed of Cu nanoparticles.[8] The addition of PTFE nanoparticles balanced the interfacial tension at the solid–liquid interface, which suppressed excessive penetration of the electrolyte into the catalyst layer, promoting CO_2 electroreduction. Inoue *et al.* successfully increased the partial current density for gaseous CO_2 reduction reactions to C_{2+} products using Cu nanoparticles. The partial current density for C_{2+} reached 1.7 A cm^{-2} with an FE of 77%.[22–24] Although the authors used ordinary components such as Cu nanoparticles and carbon-based GDEs, the high performance of their system was enabled by proper assembly.[22] Through a correlation analysis between electrochemical performance and physicochemical properties, they identified the catalyst layer thickness and the interparticle spacing in the catalyst layer as the most important parameters for enhancing the current density.[23] A moderate catalyst layer thickness and minimized interparticle spacing were found to enhance $j_{C_{2+}}$ by suppressing excessive electrolyte penetration into the catalyst layer and promoting the formation of an extensive three-phase interface.

2.2 Membrane electrode assembly (MEA) electrolyzers

Cell voltage is directly related to energy efficiency and is one of the most important parameters governing the feasibility of net-zero emissions. Most of the high-rate gaseous CO_2 electrolysis processes mentioned above were assessed in a flow cell with a liquid electrolyte (Fig. 2a). However, in practical operation, a liquid layer with a thickness of approximately 1 mm or more must be maintained, which increases the electrolyte resistance and causes a substantial IR drop under high-current-density
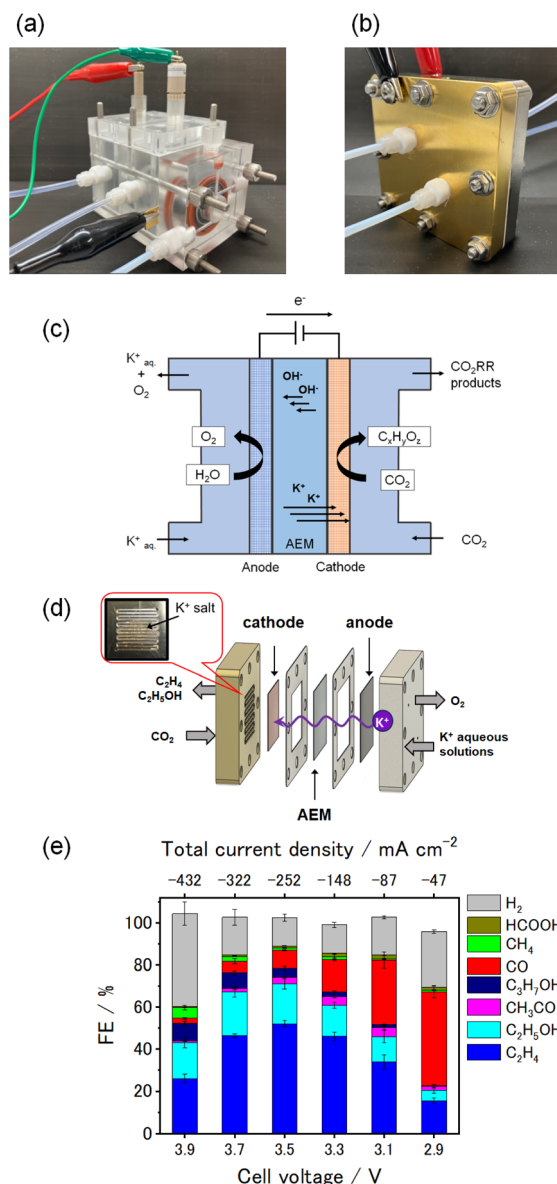

Fig. 2 Photographs of (a) the flow cell and (b) the MEA cell. (c) Cross-sectional schematic of the MEA cell. (d) Schematic of the internal structure of the MEA cell, where K^+ ions permeate through the AEM, leading to salt precipitation. (e) FEs of CO_2RR products at different cell voltages using the MEA cell.

conditions, thereby making it difficult to reduce the operating voltage. Therefore, an MEA with a minimal electrolyte thickness is considered promising for CO_2 electrolysis (Fig. 2b and c). A cation-exchange membrane (CEM) exposes the cathode to a strongly acidic medium, which substantially lowers the selectivity by promoting the HER; thus, an anion-exchange membrane (AEM) is generally selected for solid-electrolyte CO_2 electrolysis.

In 2019, Sinton *et al.* were the first to report C_{2+} production in an MEA cell using an AEM, where an electrode coated with Cu nanoparticles and a $KHCO_3$ aqueous solution (as the anolyte) achieved 78% FE for C_{2+} products at $j_{C_{2+}}$ = 200 mA cm^{-2}.[25] This work was the first demonstration of C_{2+} formation using MEA-

type electrolyzers. Subsequent progress in the design and development of catalyst and electrode architectures, together with advances in ion-exchange membrane engineering, has further led to the emergence of MEA-based electrolyzer systems with substantially enhanced catalytic activity and performance (*e.g.*, the cases presented in Table S1). In 2021, a Cu–SiO$_x$ catalyst, which was synthesized *via* one-pot coprecipitation and integrated into an MEA electrolyzer, achieved an FE as high as 65% for C$_2$H$_4$ at 215 mA cm^{-2} with stable operation over a period of 50 h.[26] Li *et al.* used quaternary ammonium poly(-ether ether ketone) (QAPEEK) as a bifunctional ionomer that conducts ions and activates CO$_2$ at the catalyst–electrolyte interface, achieving a C$_2$H$_4$ partial current density of 420 mA cm^{-2} at 3.54 V and a total current density of 1000 mA cm^{-2} at 3.73 V.[27] Lee *et al.* developed an efficient and stackable electrode design employing KOH-incorporated Cu nanoparticles (Cu–KOH) as the cathode in an MEA electrolyzer, achieving a 78.7% FE for C$_2$ products (54.5% for C$_2$H$_4$) at 281 mA cm^{-2}. *Operando* X-ray absorption spectroscopy revealed a predominantly metallic Cu state with residual oxide-derived species that synergistically promote CO$_2$-to-C$_2$H$_4$ conversion.[28]

One of the important unresolved topics related to the operating principle of CO$_2$ electrolysis using MEA cells is the ion distribution and its role. In the following, we discuss this point by comparing it with similar systems such as water electrolysis and fuel cells that also use MEA cells. In proton exchange membrane (PEM)-type water electrolysis and polymer electrolyte fuel cells (PEFCs), alkali-metal cations are typically not used. Even for AEM-type water electrolysis, symmetric ion distribution designs are generally adopted, either by using ion-exchanged membranes for both electrode solutions or by using an electrolyte containing alkali-metal cations on both sides. By contrast, AEM–MEA-type CO$_2$ electrolysis is carried out under a highly asymmetric ionic environment. A liquid electrolyte containing alkali-metal cations is supplied as the anolyte, whereas only the solid electrolyte (ionomer) exists as the ionic species on the cathode side at the beginning of electrolysis.

On the basis of the structure presented in Fig. 2d, the presence of an AEM was expected to prevent the migration of cationic species between the electrodes. Nevertheless, with such an asymmetric configuration under actual electrolysis conditions, crossover of alkali-metal cations occurred from the anode to the cathode.[29–32] After electrolysis, (bi)carbonate precipitates derived from alkali-metal cations, which were absent on the cathode side at the beginning of the reaction, were observed on the cathode end plate. The limited anion selectivity is attributable to the low density of cationic functional groups within the AEM as well as to the presence of microscopic pinholes. Kato *et al.* reported that the proportion of K$^+$ ions among the mobile ion carriers that contributed to the total current density ranged from 0.1% to 2.5%, which is sufficient to cause problematic salt precipitation.[29]

Conversely, alkali-metal cations have also been reported to promote C$_{2+}$ products formation in MEA electrolyzers. In the absence of alkali-metal cations, the cationic species present at the catalyst surface are limited to quaternary ammonium groups from the ionomer and a negligible concentration of protons. Although there are a few reports on C$_{2+}$ products

formation even in systems with pure water as the anolyte (*i.e.*, without alkali-metal cations),[27,33,34] most reports of C$_{2+}$ product formation in MEA electrolysis involve the addition of alkali-metal cations (Table S1). Kurihara *et al.* demonstrated that almost no C$_{2+}$ products were formed when large organic cations were present and alkali-metal cations were absent because their bulky structures led to a lower local cation density at the electrode surface, thereby diminishing the electric field strength within the electric double layer.[35] The weakened interfacial electric field failed to adequately stabilize key dipolar intermediates such as *CO$_2$ and *OCCO, which are essential for promoting C–C coupling toward multicarbon products. The bulky structure of quaternary ammonium groups hinders their dense alignment on the catalyst surface because of steric repulsion. Therefore, alkali-metal cations penetrating from the anolyte are typically necessary to establish a stable electric double layer in most MEA-based CO$_2$ electrolysis systems.

2.3   Stability issues in gaseous CO$_2$ electrolysis systems

Here, we summarize the key challenges associated with the stable operation of gaseous CO$_2$ electrolysis, with particular emphasis on those encountered in MEA electrolyzers. The main factors responsible for activity degradation can be broadly classified into three categories: (i) flooding and (bi)carbonate salt precipitation, (ii) chemical and mechanical degradation of the membrane, and (iii) catalyst degradation.

Among these, flooding and (bi)carbonate salt precipitation are the most widely recognized and rapidly manifest causes of performance loss in MEA electrolyzes. During electrolysis, alkali-metal cations supplied in the anolyte penetrate the membrane and reach the cathode side, as mentioned above. This cation crossover leads to progressive wetting of the GDE, disrupting the three-phase interface and increasing the fraction of two-phase catalyst–electrolyte interfaces. Simultaneously, the migrated alkali-metal cations react with CO$_2$ to form (bi)carbonate salts, which precipitate within the GDE and flow fields, thereby obstructing gas transport. This sequence of interrelated phenomena typically occurs on the shortest time scale among known degradation processes and is therefore regarded as the dominant origin of rapid activity decay in most MEA-type CO$_2$ electrolysis systems.[31,36,37] Nevertheless, the detailed mechanisms underlying flooding have not yet been fully elucidated. The acceleration of electrode hydrophilicity is generally attributed to surface charge accumulation induced by the applied potential, namely electrowetting. In contrast, Ager *et al.* reported that minor CO$_2$RR byproducts, such as acrolein, can be converted into hydrophilic poly(acrylic acid), leading to the degradation of the intrinsic hydrophobicity of GDEs.[38] Clarifying the detailed mechanisms responsible for flooding is essential for preventing this phenomenon. In addition, the causal relationship between flooding and (bi)carbonate salt precipitation remains unclear. It is still uncertain which process precedes the other, that is, whether flooding triggers salt precipitation or *vice versa*. Previous studies have reported difficulties in disentangling these two phenomena,[36,39] and this lack of clarity hampers the establishment of rational design

principles for improving the operational stability of MEA-based CO_2 electrolysis systems.

Based on insights from AEM-based water electrolysis technologies,[40,41] the limited robustness of AEMs is expected to become a critical issue. Membrane degradation not only leads to an increase in cell voltage due to reduced ionic conductivity but also, in severe cases, causes significant crossover of reactants and products, thereby hindering stable operation. In particular, AEMs have been reported to be chemically less stable than PEMs, making their durability a key challenge for future development. Quaternary ammonium cation functional groups are especially vulnerable, as they readily decompose *via* Hofmann elimination and nucleophilic attack by hydroxide ions, necessitating the molecular design of highly durable cationic structures. From the perspective of mechanical durability, membrane damage induced by carbon fibers in the GDE as well as degradation caused by non-uniform pressure distribution across the cell have also been identified as critical concerns.[42] In this regard, in addition to improving the molecular backbone, structural approaches such as reinforcing the membrane through compositing with a supporting framework are also considered effective.

Several comprehensive reviews have already addressed catalyst degradation, particularly in Cu-based systems;[43–45] therefore, detailed discussion is not repeated here. Nevertheless, catalyst degradation can proceed through a range of physical and chemical processes, including detachment, dissolution, Ostwald ripening, reshaping, and agglomeration. Although Cu is generally regarded as stable even under strongly cathodic potentials, it has been reported that even minor perturbations, such as trace oxygen contamination, can markedly accelerate degradation and surface restructuring.[46–50] For example, surface reconstruction has been shown to occur extremely rapidly when a potential is applied to Cu that has experienced open-circuit conditions or slight air oxidation, leading to the formation of oxygen-containing surface species.[49] In addition, multiple studies have demonstrated that Cu dissolution is significantly enhanced under CO_2 electrolysis conditions compared with inert Ar atmospheres. This enhanced dissolution has been attributed to the formation of Cu–carbonyl complexes with CO, a CO_2 reduction product, which facilitates metal dissolution.[50]

Importantly, despite the existence of multiple degradation pathways, only issues that manifest on very short time scales, such as salt precipitation, have been prominently observed to date. As a consequence, other degradation mechanisms and the corresponding mitigation strategies have not yet been examined in sufficient detail. Therefore, resolving salt precipitation, which occurs on short time scales, should be regarded as the highest priority. This necessitates the complete elimination of free alkali cations in AEM–MEA CO_2 electrolysis systems. The details of this strategy are discussed in Section 4.

3 Life-cycle assessment for CO_2 electrolysis

Recent advancements in electrodes, such as catalysts and GDEs, as well as electrolyzers, including MEA and AEM, were introduced in the previous section. Although numerous cutting-edge technologies have been developed for converting CO_2 into valuable chemicals, comprehensively evaluating CO_2 emissions in the entire system is essential because this system entails a large amount of electricity.

As mentioned above, Yamaguchi *et al.* recently evaluated the electrochemical reduction of CO_2 to C_2H_4 on the basis of the prospective LCA.[19] A schematic of the system boundary is shown in Fig. 3. CO_2 directly captured from the air using direct air capture (DAC) technology[51] is fed into electrochemical CO_2 reduction (eCO_2R) devices to produce C_2H_4. The outlet flow from the eCO_2R system contains the product (*i.e.*, C_2H_4), unreacted CO_2, and byproducts (*i.e.*, H_2, CO, and CH_4) because the conversion is set at 20% in the study.[19] Gaseous byproducts that include unreacted CO_2 and liquid byproducts were separated using a vapor–liquid (VL) separation system. Through an electrochemical CO_2 enrichment (eCO_2E) process,[52–56] unreacted CO_2 is captured and recycled to the eCO_2R system. The obtained C_2H_4 is purified as a final product by removing gas byproducts using the cryogenic separation ("Cryogenic" in Fig. 3) process. All of the byproducts are burnt in an incinerator ("Incinerator" in Fig. 3), and the generated heat is supplied to the DAC system *via* a heat exchanger while CO_2 in the flue gas is recycled to the DAC system. Importantly in eCO_2R, some CO_2
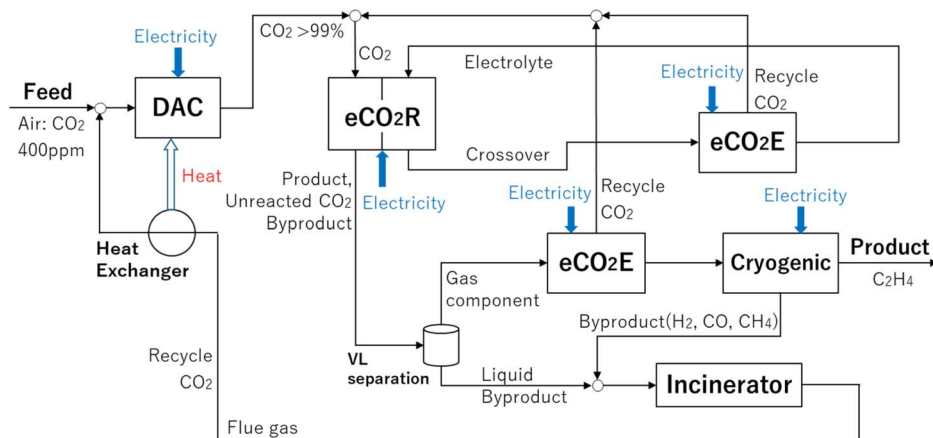

Fig. 3 Schematic of the system boundary for CO_2 reduction.

molecules move to the counter electrode (referred to as crossover CO_2). In basic or neutral electrolytes, dissolved CO_2 molecules migrate from the cathode side to the anode side in the form of (bi)carbonate species.[57–59] Another eCO_2E system is installed to recover the crossover CO_2 and recycle it to the eCO_2R system. In the evaluation, five devices are considered in total (DAC, eCO_2R, eCO_2E, Cryogenic, and Incinerator). In this case, the cell voltage is 3.5 V, the FE is 70%, and the conversion is 20%. These are the key data in the publication.[19] The authors assumed that the power from renewable energy sources (0.032 kg_{-CO_2e} kWh^{-1}) was used in the study.[19,60] They identified six key performance indicators that include cell voltage, FE, conversion, enrichment cell voltage, current density, and consumables lifetime, which have a large impact on CO_2 emissions. They also evaluated several scenarios and pointed out that the net CO_2 emission can be down to 0.4 kg_{-CO_2e} $kg_{-C_2H_4}^{-1}$.

Our group also conducted electrochemical reduction of CO_2 to C_2H_4 using MEA electrolyzers as reported in a recent publication (Fig. 2e), with details of the materials and electrolysis conditions provided in Note S1 and Fig. S1.[29] The MEA electrolyzer allows lowering the cell voltage compared to conventional electrolyzers. The current density proportionally increases from 470 to 4320 A m^{-2} as the cell voltage rises from 2.9 to 3.9 V. Under this operation, the conversion, defined based on the amount of CO_2 consumed, increases up to approximately 6.4% at 3.7 V and gradually decreases to 5.9% at 3.9 V. Concurrently, the hydrogen production increases with higher cell voltage (ca. 44% at 3.9 V). While FE distinctly varies with the cell voltage, the highest FE of 52% is achieved at the cell voltage of 3.5 V (summarized in Table 1). We employed the above-mentioned method[19] to evaluate our experimental data and estimate CO_2 emissions of the system. By closely following the reported method,[19] we simulated the electricity consumption of the system (DAC, eCO_2R, eCO_2E, Cryogenic, and Incinerator) and evaluated CO_2 emissions using a power with the emission factor of 0.032 kg_{-CO_2e} kWh^{-1}. In addition, eCO_2E is not installed after DAC system in the present evaluation because the purity of CO_2 after DAC is assumed to be sufficiently high (>99%). The results are summarized in Fig. 3.

As seen in Fig. 4, the major contribution of CO_2 emissions results from eCO_2E and eCO_2R. In the figure, negative CO_2 emission values indicate the amount of CO_2 used for C_2H_4

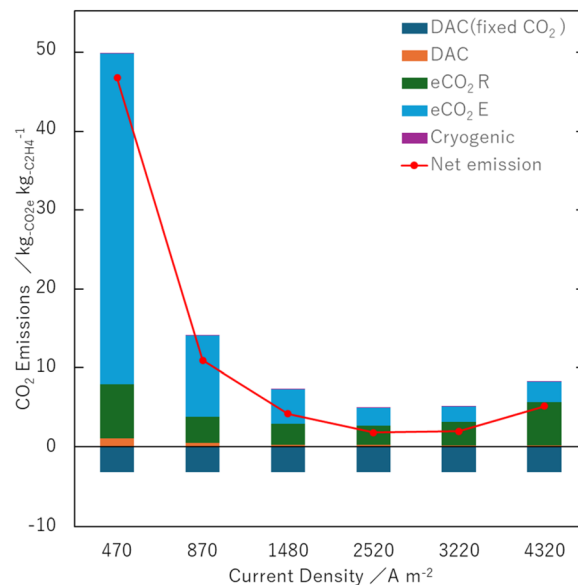**Fig. 4** The CO_2 emissions of the eCO_2R system with a MEA electrolyzer.

production while the net emissions are represented by red dots. The net emission ranges from 1.8 kg_{-CO_2e} $kg_{-C_2H_4}^{-1}$ at 3.5 V to 46 kg_{-CO_2e} $kg_{-C_2H_4}^{-1}$ at 2.9 V, which is higher than that in the previous reports.[19,61] The contributions from DAC and Cryogenic are relatively small, although their energy consumption values are not negligible (0.70 kWh $kg_{-CO_2}^{-1}$ captured, 1.3 kWh $kg_{-C_2H_4}^{-1}$).[19,51] It is partially because some heat recycled in Incinerator is supplied to DAC. Nonetheless, it is indicated that the electricity consumption of eCO_2E and eCO_2R is markedly large.

CO_2 emissions from eCO_2E are considerably higher than those reported in the previous case.[19] This is primarily due to the low conversion in the present case. While the previous study assumed a conversion of 20%, the actual conversion in this work ranges from 1.5% to 6.4%. This results in a significant amount of unreacted CO_2 that needs to be captured with eCO_2E, leading to a large amount of CO_2 emissions. This is the primary reason why the net CO_2 emissions in our case are higher than those in the previous report.[19] In addition, they also mentioned

Table 1 Summary of key parameters and experimental results reported for the MEA electrolyzer used in the LCA calculation[29]

Cell voltage [V]	Current density [A m^{-2}]	Supplied electricity [kW m^{-2}]	FE (C_2H_4) [%]	FE (H_2) [%]	CO_2 conversion[a] [%]	C_2H_4 yield[b] [%]	Electricity [kWh $kg_{-C_2H_4}^{-1}$]
2.9	470	1.4	15.5	26.5	1.5	0.1	214.3
3.1	870	2.7	34.1	18.0	2.6	0.6	104.4
3.3	1480	4.9	46.1	13.5	3.5	1.4	82.1
3.5	2520	8.8	52.2	13.5	5.5	2.6	77.0
3.7	3220	11.9	46.5	18.0	6.4	3.0	91.3
3.9	4320	16.9	26.0	44.1	5.9	2.2	171.8

[a] The proportion of feed CO_2 converted into any products (H_2, CO, CH_4, C_2H_4, C_2H_5OH and so on). [b] C_2H_4 yield was determined by dividing the C_2H_4 production rate by the CO_2 flow rate. In the previous study,[29] the CO_2 flow rate was fixed at 314 mol m^{-2} h^{-1}. The production rate was calculated from the product of the current density, FE (C_2H_4), and the carbon number (2) divided by the electron transfer number (12) and the Faraday constant.

that CO_2 emissions in eCO_2E significantly increase at a conversion lower than 20%.[19]

Therefore, it is pivotal to gain the conversion to reduce CO_2 emissions in eCO_2E. One may speculate that the conversion can be increased by adjusting experimental conditions (e.g., CO_2 flow rate into eCO_2R). However, such optimization is not straightforward, as variations in these parameters influence multiple factors, including the FE of the product (discussed in the next section). More importantly, it may be needed to increase the reaction rate and also to further improve the electrolyzer structure to gain high conversion. In addition to the conversion, if the eCO_2E cell voltage is decreased, it directly has an impact on mitigating CO_2 emissions.[52] Overall, the conversion has a significant impact on CO_2 emissions from eCO_2E. Moreover, the eCO_2E process is also used to recover crossover CO_2 in the counter electrode, besides CO_2 unreacted through eCO_2R. In this evaluation, the amount of crossover CO_2 is assumed to be a half of the hydroxide ions, following the previous publication.[19] Based on this assumption, while one molecule of C_2H_4 is produced, 12 moles of hydroxide ions are generated; in turn, 6 moles of CO_2 are assumed to move from the cathode side to the anode side, which cannot be ignorable. It would be desired to hinder crossover CO_2 in eCO_2R by improving electrolytes such as the addition of chemicals.

The operating conditions of eCO_2R play a critical role in determining overall CO_2 emissions. In most reported systems (e.g., the cases presented in Table S1), the cell voltage for MEA electrolyzers ranges from approximately ~3 to ~4 V. For example, in the case of C_2H_4 production, the reduction of one CO_2 molecule involves a six-electron transfer, and such a high cell voltage leads to significant electricity consumption. It should be noted that the excess voltage results in dissipating as heat and ending up a large amount of CO_2 emission. Therefore, minimizing the excess voltage is essential to lower CO_2 emissions. In the current case, the use of an MEA-based cell allows a significant reduction in cell voltage (below 4 V) compared to other types of cells; however, the voltage remains relatively high. Second, as the cell voltage increases, the current density also increases. Although the current density does not directly affect CO_2 emissions, it influences the system throughput. If the current density is low, a larger number of electrolyzers must be installed to maintain the desired C_2H_4 production rate. Consequently, a trade-off relationship exists between CO_2 emissions caused by excess cell voltage and equipment cost that stems from the number of electrolyzers. The equipment cost cannot be precisely evaluated because its unit price is not fixed, which remains a challenge for implementing this technology in practical applications in the future. Finally, the cell voltage is tightly correlated to FE. Indeed, FE for C_2H_4 is approximately 15% at cell voltage equal to 2.9 V; it increases up to about 52% at 3.5 V. If the FE for CO_2 reduction decreases and H_2 production increases, additional energy is consumed without contributing to CO_2 fixation. Moreover, since the byproducts are incinerated, they are directly related to CO_2 emissions. Therefore, it is crucial to minimize byproducts to achieve high FE.

The lifetime of electrolyzers influences both the LCA outcomes and the equipment cost. As discussed in the previous section, the lifetime is closely linked to the stability of the electrolyzers. A short lifetime can significantly affect both the LCA and the cost. However, following the assumptions in the previous study (the lifetimes exceed 8000 hours for consumables and 20 years for construction materials), these impacts are insignificant.[19]

Overall, a quite complex relationship exists between the cell voltage, the current density, and FE, which makes it challenging to identify optimal operating conditions and lead the development of electrolyzers. In fact, even when the same electrolyzer was used, CO_2 emissions dramatically vary depending on operating conditions. It is equally important to find out the optimum condition and develop a new electrolyzer. The structure and type of electrodes, catalysts, and electrolyzers should be evaluated under these optimal conditions to meet the performance requirements. Based on these LCA results, the future prospects of CO_2 electrolysis technology for achieving negative emissions are discussed in the next section.

4 Challenges of CO_2 electrolysis technologies for achieving negative emissions

4.1 Improvement of single-pass CO_2 conversion

As discussed in the previous section, one of the most critical criteria for achieving negative emissions is the CO_2 conversion. As described above, a low CO_2 conversion substantially increases the energy required for recycling unconverted CO_2. However, two points must be noted here. First, although a higher CO_2 conversion undoubtedly expands the operating window for achieving negative emissions and maximizing the conversion is desirable, in practice, a conversion of ~20% is sufficient to achieve negative emissions. Therefore, it is necessary to set appropriate benchmarks that consider the balance with other parameters. Second, many previous studies (e.g., the cases presented in Table S1) used reaction conditions that included an excessive supply of CO_2, resulting in situations where enhancing the CO_2 conversion was not actively pursued. Consequently, the CO_2 conversion values reported in the literature do not necessarily reflect the maximum achievable conversion for those systems.

To enhance CO_2 conversion, particularly the single-pass conversion efficiency, it is necessary to (i) achieve a high FE for CO_2 reduction under a low CO_2 partial pressure and (ii) effectively suppress CO_2 crossover from the cathode to the anode. For (i), when CO_2 is diluted by final products or inert gases, such as H_2 and C_2H_4, the FE for C_{2+} products on Cu-based catalysts is known to decrease substantially. For instance, Oh et al. reported that the FE for C_{2+} decreased from 61% to 34% when the CO_2 concentration was reduced from 75% to 25% at a low flow rate.[62] Therefore, it is necessary to consider strategies such as designing catalysts that can increase CO_2 adsorption even under a low CO_2 partial pressure or increasing the proportion of liquid products (e.g., ethanol), to mitigate the dilution of CO_2 by gaseous products.[63]

For (ii) suppressing CO_2 crossover, one solution is to use a CEM to block the crossover of (bi)carbonate anions. An MEA based on a bipolar membrane (BPM) is a promising configuration because it suppresses local acidification, which favors the HER while also preventing HCO_3^- crossover (Fig. 5a). For example, She *et al.* developed a pure-water-fed bipolar-type MEA electrolyzer in which an AEM and a PEM are laminated to form an internal acid–base junction that suppresses CO_3^{2-} formation and CO_2 crossover, enabling over 1000 h of stable operation at 333 mA cm^{-2} with 50% FE for C_2H_4.[33] Alternatively, CO_2 reduction using HCO_3^--derived CO_2 is another effective approach to suppress CO_2 crossover using a CEM (Fig. 5b).[64–66] A HCO_3^- or CO_3^{2-} aqueous solution is supplied to the cathode chamber, whereas pure water or an acidic aqueous solution without alkali-metal cations is supplied to the anode chamber. The OER proceeds at the anode, and H^+ ions are transported to the cathode side through the CEM. Gaseous CO_2 is subsequently generated *in situ* within the electrolyzer *via* an acid–base reaction between the H^+ ions and the (bi)carbonate ions. The buffering layer serves as the region where this gaseous CO_2 is produced. The generated CO_2 is then directly delivered to the cathode, enabling the *in situ* formation of the three-phase interface. For example, Berlinguette *et al.* demonstrated that, in a flow cell equipped with a BPM and a Ag nanoparticle catalyst on a porous carbon support, aqueous 3.0 M $KHCO_3$ solutions can be electrochemically converted into CO gas without the supply of external CO_2, achieving FEs of 81% at 25 mA cm^{-2} and 37% at 100 mA cm^{-2}.[64] Zhang *et al.* used a CEM as the separator and a redox-active polymer network incorporating Cu as the cathode catalyst while feeding a 1 M K_2CO_3 aqueous

solution to the cathode chamber. Under these conditions, they achieved a C_{2+} FE of 55% at a total current density of 300 mA cm^{-2}, with C_2H_4 constituting 56 wt% of the outlet gas stream.[65]

4.2 Reduction of cell voltage

Another key parameter to achieve negative emission is the cell voltage. Although most recent reports describe cell voltages in the range from ~3 to ~4 V in AEM-based CO_2 electrolysis (Table S1), the specific contributions of each voltage component have not been fully elucidated. Potential deconvolution is essential for identifying strategies for further voltage reduction. Weng *et al.* demonstrated the breakdown of cell voltage in MEA electrolyzers with Cu-based catalysts.[67,68] Among the various overpotentials, the cathodic overpotential was the dominant contributor. Cathodic overpotentials of approximately 0.5 to 1.0 V were required, even at current densities ranging from 100 to 250 mA cm^{-2}. He *et al.* have reported similar findings in MEA systems, where cathodic overpotentials in the range of 0.5–1.0 V were experimentally observed.[69] Such large cathodic overpotentials contrast sharply with those observed in water electrolysis, where the HER proceeds with a low cathodic overpotential. For instance, in AEM-based MEA water electrolyzers, cathodic overpotentials remain below 0.1 V even at current densities exceeding 1 A cm^{-2}. In the case of PEM-based MEA water electrolysis, the cathodic overpotentials are nearly zero even at higher current densities.[70] These unusually high cathodic overpotentials in the CO_2RR represent a major limitation to the overall energy efficiency of the process compared with that of water electrolysis.

We now consider the cathodic overpotential in greater detail. As previously mentioned, reducing the large overpotential associated with the transformation of CO_2 molecules (*i.e.*, the reaction overpotential) requires the development of novel catalyst materials. As stated in the Introduction, detailed discussions on catalyst materials and the molecular-level mechanism of CO_2 transformation are beyond the scope of this paper. However, we emphasize again that researchers should recognize the importance of reaction overpotential. When developing electrocatalysts for fuel cells or water electrolyzers, the reaction overpotential is generally considered the most important parameter. By contrast, for the CO_2RR, product selectivity is often discussed as the most critical parameter. However, LCA analyses indicate that, if the reaction overpotential is substantially reduced, a catalyst can still be practically applicable even with a somewhat lower FE.

In addition to reducing the reaction overpotential through catalyst design, minimizing Nernstian loss associated with the pH gradients and diffusion overpotential is also an effective strategy for lowering the cathodic overpotential. The local pH of the cathode surface reached approximately 14 at 300 mA cm^{-2} because of proton consumption in the presence of alkali-metal cations.[71] When neutral anolytes were used, the pH gradient was 6–7, leading to a Nernstian loss of 0.3–0.4 V. Importantly, this increase in the local pH leads to a higher cell voltage (*i.e.*, larger Nernstian loss), but at the same time, it suppresses the HER, which is beneficial for improving product selectivity. Therefore,

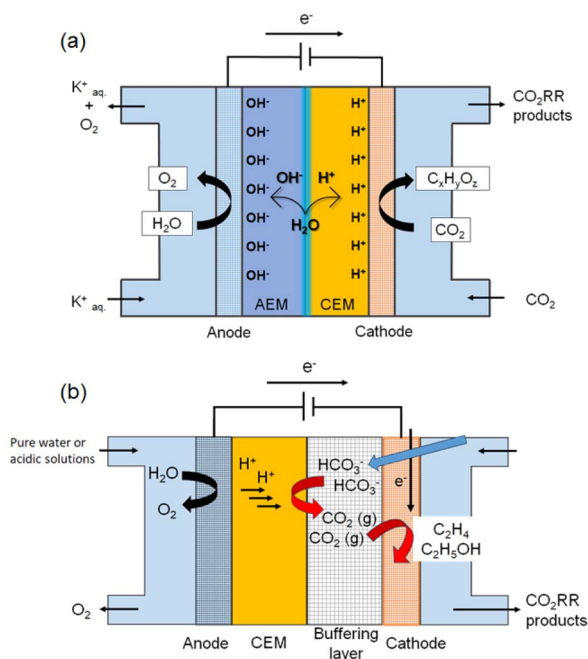**Fig. 5** Configurations for suppressing CO_2 crossover: (a) a BPM-based MEA with an internal acid–base junction and (b) a bicarbonate-derived CO_2 electrolysis system with a CEM enabling *in situ* CO_2 generation at the three-phase interface.

an appropriate balance between enhancing selectivity and minimizing voltage loss must be achieved by precisely controlling the local pH. Several strategies, such as introducing a buffer layer or controlling the water content, have been proposed to control local pH.[72,73]

4.3 Enhancement of operational stability

The stability of the system influences both the LCA outcomes and the costs, particularly capital expenditures. Because reliable unit prices of electrolyzers and their consumables are not available, this issue was not examined in detail in the preceding sections. Nevertheless, it is evident that ensuring stable operation is crucial for reducing capital costs. As discussed above, the highest-priority stability issue is salt precipitation on very short time scales. Therefore, the development of pure-water-fed MEA systems that suppress salt precipitation is highly desirable. Although pure-water-fed MEA electrolyzers provide a rational solution to mitigate salt precipitation that limits stable operation, general design principles for achieving C_{2+} product formation using AEMs under alkali-cation-free conditions have not yet been established. Our proposed strategy for achieving C_{2+} product formation in pure-water-fed AEM-based systems can be broadly divided into two approaches, or a combination of both. One approach focuses on electrolyte engineering to control the electric double layer, while the other relies on catalyst design to lower the activation energy for C_{2+} formation.

From the perspective of electrolyte engineering, as discussed above, smaller cations tend to accumulate more readily at the catalyst surface, resulting in a stronger interfacial electric field within the electric double layer and thereby promoting C_{2+} product formation.[35,74–76] For this interfacial electric field effect, a key challenge in employing ionomers to generate a sufficiently strong interfacial electric field is how to achieve a high interfacial density of cationic species. Specifically, reducing the steric bulk of quaternary ammonium cation functionalities, while simultaneously enhancing the hydrophilic/hydrophobic contrast between the side chains and the polymer backbone,

would increase the local cation density by promoting more distinct phase separation into hydrophilic and hydrophobic domains.[77–80] Furthermore, based on the previous studies on fuel cells, the ionomer deposition protocol and subsequent drying processes can substantially modify the resulting domain morphology.[81,82] These observations highlight that process-level control over interface formation is as critical as molecular design in establishing favorable interfacial structures.

Beyond the interfacial electric field effect, alkali-metal cations have also been proposed to stabilize C_2 intermediates through direct coordination. However, such a coordination effect would be very limited for quaternary ammonium cations owing to their low Lewis acidity.[35,83] Consequently, under pure-water-fed conditions, the stabilization of reaction intermediates must rely primarily on the intrinsic properties of the catalyst surface. In the absence of alkali-metal cations, interactions between the catalyst surface and reaction intermediates are therefore expected to exert a more pronounced influence on reaction behavior than in alkali-cation-containing systems. This perspective implies that catalyst design principles developed under alkali-cation-containing conditions may not be directly transferable to pure-water-fed AEM-based CO_2 electrolysis.

Further, a pure-water-fed CEM-MEA electrolyzer can be regarded as an ultimate configuration that simultaneously mitigates Nernstian losses while resolving issues such as salt precipitation and CO_2 crossover. This system is conceptually analogous to PEFCs and PEM water electrolyzers, and therefore holds strong potential from the perspectives of component reliability and practical implementation. However, in a pure-water-fed CEM-MEA electrolyzer, the local pH near the cathode surface becomes highly acidic. Under such conditions, achieving efficient CO_2 reduction while suppressing the HER necessitates a significant breakthrough in the development of electrocatalysts that can maintain CO_2RR activity under acidic environments.

In parallel, numerous efforts are underway to improve the operational stability of CO_2 electrolysis systems employing alkaline-cation-containing electrolytes, and such systems may
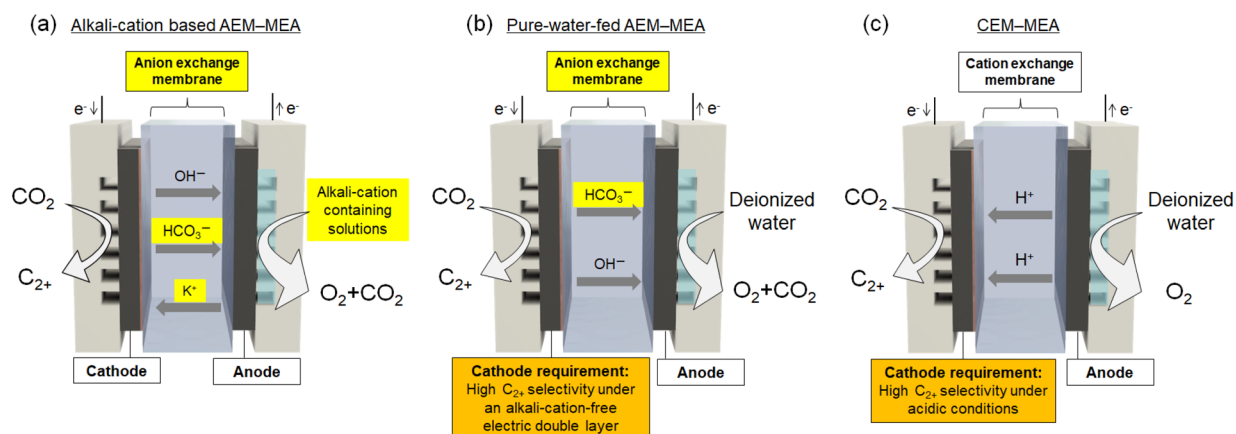

Fig. 6 Schematic comparison of three MEA configurations for CO_2 electrolysis: (a) alkali-cation-based AEM−MEA, (b) pure-water-fed AEM−MEA, and (c) CEM−MEA. Components and phenomena that require improvement are highlighted in yellow, while the requirements for the cathode electrocatalyst are highlighted in orange.

reach societal implementation earlier than pure-water-fed configurations. To address the challenge of salt precipitation inherent to these systems, several mitigation strategies have been explored, including pulsed electrolysis to promote repeated salt precipitation and dissolution,[84,85] feedback control of alkali-metal cation concentrations to extend operational lifetimes,[29,86] and periodic washing protocols to remove accumulated salts.[87,88] Although these approaches do not fundamentally resolve salt precipitation, they represent critically important interim solutions for accelerating societal implementation.

5 Conclusion and outlook

LCA is the essential analytical framework for guiding the advancement of CO_2 electrolysis technology toward practical and industrial implementation. These quantitative assessments clarify the correlations between total system energy consumption and greenhouse gas emissions, thereby identifying the key technological targets required to achieve negative emissions. Meeting these benchmarks requires not only the rational design of electrode catalysts but also the optimization and coordinated operation of macroscopic components such as electrodes, electrolytes, and electrolyzer configurations. The development of GDEs has enabled ampere level current densities through the optimized construction of the three-phase interface. MEA electrolyzers offer a promising configuration that enables low-voltage and high-current-density operation by minimizing the electrolyte layer thickness. Nevertheless, AEM-based MEAs suffer from alkali-metal cation crossover due to asymmetric ion distributions, which leads to gradual performance degradation.

The anticipated pathway toward the practical deployment of MEA-based electrolyzers equipped with GDEs is outlined as follows. First, MEA electrolyzers or zero-gap electrolyzers employing alkali-metal cations in the anolyte, which represent the current standard configuration, are expected to be commercialized initially (Fig. 6a). In such systems, flooding and salt precipitation are anticipated to be managed through operational strategies, including periodic salt removal and feedback control of the alkali-metal cation concentration. Indeed, recent studies have already demonstrated relatively long-term stable operation by implementing these approaches.[29,84,86] The next stage is expected to involve the social implementation of alkali-cation-free AEM-based MEA electrolysis, as discussed in Section 4 (Fig. 6b). If interface engineering and catalyst optimization enable the formation of an electric double layer that does not rely on alkali-metal cations, the system can be freed from issues arising from asymmetric ion distributions. Looking further ahead, an alkali-cation-free acidic MEA configuration employing a robust CEM, analogous to PEM water electrolyzers and PEFCs, can be envisioned (Fig. 6c). Owing to the ability to resolve the inherent weaknesses AEMs, as well as the issues of CO_2 (carbonate) crossover, this approach can be regarded as the ultimate CO_2 electrolysis system conceivable at present. However, its realization requires a major breakthrough in the development of electrocatalysts that can suppress hydrogen evolution while promoting CO_2 electrolysis at the cathode under acidic conditions.

LCA indicates that reducing the cell voltage and improving the single-pass conversion are the most effective means to minimize greenhouse gas emissions and approach negative emission conditions. In particular, the reaction overpotential associated with CO_2 molecular conversion and the Nernstian loss caused by pH gradients are the primary factors that increase the cell voltage, and must be mitigated through advanced materials design and interface engineering. Enhancing the single-pass conversion requires suppressing CO_2 crossover and optimizing the reaction environment to maintain a high conversion efficiency even under dilute CO_2 conditions, thereby reducing the energy consumption of CO_2 enrichment processes. Recently, BPM-based MEAs and bicarbonate-derived CO_2 electrolyzers that enable *in situ* CO_2 generation have been proposed as next-generation systems that combine high energy efficiency and durability.

Future progress will rely on integrating nanoscale catalyst design with macroscale electrode and electrolyzer engineering, guided by continuous evaluation based on LCA. Establishing such a multiscale and quantitative design framework will enable CO_2 electrolysis to evolve from laboratory research into an industrial carbon circular technology capable of realizing sustainable negative emission manufacturing.

Author contributions

K. K. and S. K.: conceptualization, manuscript drafting and writing; S. Nakasone, R. K., A. I. and H. I.: literature collection, partial manuscript drafting and writing; S. Nakahata: reference collection, editing and writing; Y. N.: discussion, revision; S. T. and T. T. H. N.: data analysis; all authors: approval of the final manuscript.

Conflicts of interest

There are no conflicts to declare.

Data availability

The data that support the findings of this study are available from the corresponding author upon reasonable request.

Supplementary information (SI) is available. See DOI: https://doi.org/10.1039/d5sc08419a.

Acknowledgements

References

1 IEA, *Global Energy Review 2025*, Paris, 2025.
2 G. Wang, J. Chen, Y. Ding, P. Cai, L. Yi, Y. Li, C. Tu, Y. Hou, Z. Wen and L. Dai, *Chem. Soc. Rev.*, 2021, **50**, 4993–5061.

3 A. R. Woldu, Z. Huang, P. Zhao, L. Hu and D. Astruc, *Coord. Chem. Rev.*, 2022, **454**, 214340.

4 Y. Ding, J. R. Bertram, C. Eckert, R. R. Bommareddy, R. Patel, A. Conradie, S. Bryan and P. Nagpal, *J. Am. Chem. Soc.*, 2019, **141**, 10272–10282.

5 E. Sediva, A. J. Carrillo, C. E. Halloran and J. L. M. Rupp, *ACS Appl. Energy Mater.*, 2021, **4**, 1474–1483.

6 Y. Kuramochi, O. Ishitani and H. Ishida, *Coord. Chem. Rev.*, 2018, **373**, 333–356.

7 S. Jin, Z. Hao, K. Zhang, Z. Yan and J. Chen, *Angew. Chem., Int. Ed.*, 2021, **60**, 20627–20648.

8 Z. Xing, L. Hu, D. S. Ripatti, X. Hu and X. Feng, *Nat. Commun.*, 2021, **12**, 136.

9 T. Burdyny and W. A. Smith, *Energy Environ. Sci.*, 2019, **12**, 1442–1453.

10 Y. Hori, A. Murata and R. Takahashi, *J. Chem. Soc., Faraday Trans. 1*, 1989, **85**, 2309–2326.

11 Y. Hori, K. Kikuchi, A. Murata and S. Suzuki, *Chem. Lett.*, 1986, **15**, 897–898.

12 Y. Hori, K. Kikuchi and S. Suzuki, *Chem. Lett.*, 1985, **14**, 1695–1698.

13 Y. Hori, H. Wakebe, T. Tsukamoto and O. Koga, *Electrochim. Acta*, 1994, **39**, 1833–1839.

14 D. F. Gao, R. M. Arán-Ais, H. S. Jeon and B. Roldan Cuenya, *Nat. Catal.*, 2019, **2**, 198–210.

15 Y. Wang, J. Liu and G. Zheng, *Adv. Mater.*, 2021, **33**, e2005798.

16 M. Li, H. Wang, W. Luo, P. C. Sherrell, J. Chen and J. Yang, *Adv. Mater.*, 2020, **32**, e2001848.

17 P. Christopher, Choosing Impactful Perspectives for Energy Research: A Case Study of CO$_2$ Electroreduction, *ACS Energy Lett.*, 2024, **9**, 5539–5540.

18 A. K. Sahu, T. E. Rufford, S. H. Ali, R. Knibbe, S. Smart, F. Jiao, A. T. Bell and X. Zhang, *Chem. Sci.*, 2025, **16**, 5819–5835.

19 S. Yamaguchi, E. Amasawa, H. Ebe, M. Hirao and M. Sugiyama, *ChemSusChem*, 2025, **18**, e202401409.

20 Y. Wu, H. Rabiee, X. S. Zhao, G. Wang and Y. Jiang, *J. Mater. Chem. A*, 2024, **12**, 14206–14228.

21 F. P. Garcia de Arquer, C. T. Dinh, A. Ozden, J. Wicks, C. McCallum, A. R. Kirmani, D. H. Nam, C. Gabardo, A. Seifitokaldani, X. Wang, Y. C. Li, F. Li, J. Edwards, L. J. Richter, S. J. Thorpe, D. Sinton and E. H. Sargent, *Science*, 2020, **367**, 661–666.

22 A. Inoue, T. Harada, S. Nakanishi and K. Kamiya, *EES Catal.*, 2023, **1**, 9–16.

23 A. Inoue, S. Nakasone, R. Yoshida, S. Nakahata, T. Harada, S. Nakanishi and K. Kamiya, *Small*, 2025, **21**, e2500693.

24 S. Nakasone, A. Inoue, R. Kurihara, H. Irie, T. Harada, S. Nakanishi and K. Kamiya, *ACS Appl. Energy Mater.*, 2025, **8**, 16802–16810.

25 C. M. Gabardo, C. P. O'Brien, J. P. Edwards, C. McCallum, Y. Xu, C.-T. Dinh, J. Li, E. H. Sargent and D. Sinton, *Joule*, 2019, **3**, 2777–2791.

26 J. Li, A. Ozden, M. Wan, Y. Hu, F. Li, Y. Wang, R. R. Zamani, D. Ren, Z. Wang, Y. Xu, D. H. Nam, J. Wicks, B. Chen, X. Wang, M. Luo, M. Graetzel, F. Che, E. H. Sargent and D. Sinton, *Nat. Commun.*, 2021, **12**, 2808.

27 W. Li, Z. Yin, Z. Gao, G. Wang, Z. Li, F. Wei, X. Wei, H. Peng, X. Hu, L. Xiao, J. Lu and L. Zhuang, *Nat. Energy*, 2022, **7**, 835–843.

28 W. H. Lee, C. Lim, S. Y. Lee, K. H. Chae, C. H. Choi, U. Lee, B. K. Min, Y. J. Hwang and H.-S. Oh, *Nano Energy*, 2021, **84**, 105859.

29 S. Kato, S. Ito, S. Nakahata, R. Kurihara, T. Harada, S. Nakanishi and K. Kamiya, *ChemSusChem*, 2024, **17**, e202401013.

30 G. A. El-Nagar, F. Haun, S. Gupta, S. Stojkovikj and M. T. Mayer, *Nat. Commun.*, 2023, **14**, 2062.

31 S. Garg, Q. Xu, A. B. Moss, M. Mirolo, W. Deng, I. Chorkendorff, J. Drnec and B. Seger, *Energy Environ. Sci.*, 2023, **16**, 1631–1643.

32 H. Simonson, D. Henckel, W. E. Klein, K. C. Neyerlin and W. A. Smith, *ACS Sustainable Chem. Eng.*, 2025, **13**, 823–833.

33 X. She, L. Zhai, Y. Wang, P. Xiong, M. M.-J. Li, T.-S. Wu, M. C. Wong, X. Guo, Z. Xu, H. Li, H. Xu, Y. Zhu, S. C. E. Tsang and S. P. Lau, *Nat. Energy*, 2024, **9**, 81–91.

34 L. Xue, Z. Gao, T. Ning, W. Li, J. Li, J. Yin, L. Xiao, G. Wang and L. Zhuang, *Angew. Chem., Int. Ed.*, 2023, **62**, e202309519.

35 R. Kurihara, S. Ito, S. Kato, T. Harada, S. Nakanishi and K. Kamiya, *EES Catal.*, 2025, **3**, 1055–1061.

36 M. Sassenburg, M. Kelly, S. Subramanian, W. A. Smith and T. Burdyny, *ACS Energy Lett.*, 2023, **8**, 321–331.

37 A. B. Moss, S. Garg, M. Mirolo, C. A. Giron Rodriguez, R. Ilvonen, I. Chorkendorff, J. Drnec and B. Seger, *Joule*, 2023, **7**, 350–365.

38 M. K. Kovalev, H. Ren, M. Zakir Muhamad, J. W. Ager and A. A. Lapkin, *ACS Energy Lett.*, 2022, **7**, 599–601.

39 K. Yang, R. Kas, W. A. Smith and T. Burdyny, *ACS Energy Lett.*, 2021, **6**, 33–40.

40 C. G. Arges, V. K. Ramani and P. N. Pintauro, *Electrochem. Soc. Interface*, 2010, **19**, 31.

41 J. R. Varcoe, P. Atanassov, D. R. Dekel, A. M. Herring, M. A. Hickner, P. A. Kohl, A. R. Kucernak, W. E. Mustain, K. Nijmeijer, K. Scott, T. Xu and L. Zhuang, *Energy Environ. Sci.*, 2014, **7**, 3135–3191.

42 C. D. Sewell, D. A. Henckel and M. G. Resch, *Ind. Eng. Chem. Res.*, 2025, **64**, 20431–20440.

43 S. Popović, M. Smiljanić, P. Jovanovič, J. Vavra, R. Buonsanti and N. Hodnik, *Angew. Chem., Int. Ed.*, 2020, **59**, 14736–14746.

44 H. Wu, H. Yu, Y.-L. Chow, P. A. Webley and J. Zhang, *Adv. Mater.*, 2024, **36**, 2403217.

45 J. Kok, P. P. Albertini, J. Leemans, R. Buonsanti and T. Burdyny, *Nat. Rev. Mater.*, 2025, **10**, 550–563.

46 D. Takamatsu, N. Fukatani, A. Yoneyama, T. Hirano, K. Hirai, S. Yabuuchi, K. Watanabe, K. Kamiya and S. Nakanishi, *J. Am. Chem. Soc.*, 2025, **147**, 24103–24112.

47 J. Kok, J. de Ruiter, W. van der Stam and T. Burdyny, *J. Am. Chem. Soc.*, 2024, **146**, 19509–19520.

48 R. Kas, K. Yang, D. Bohra, R. Kortlever, T. Burdyny and W. A. Smith, *Chem. Sci.*, 2020, **11**, 1738–1749.

49 S. J. Raaijman, N. Arulmozhi and M. T. M. Koper, *ACS Appl. Mater. Interfaces*, 2021, **13**, 48730–48744.

50 Y. Yang, J. Feijóo, M. Figueras-Valls, C. Chen, C. Shi, M. V. Fonseca Guzman, Y. Murhabazi Maombi, S. Liu, P. Jain, V. Briega-Martos, Z. Peng, Y. Shan, G. Lee, M. Rebarchik, L. Xu, C. J. Pollock, J. Jin, N. E. Soland, C. Wang, M. B. Salmeron, Z. Chen, Y. Han, M. Mavrikakis and P. Yang, *Nat. Catal.*, 2025, **8**, 579–594.

51 S. Deutz and A. Bardow, *Nat. Energy*, 2021, **6**, 203–213.

52 C. Huang, C. Liu, K. Wu, H. Yue, S. Tang, H. Lu and B. Liang, *Energy Fuels*, 2019, **33**, 3380–3389.

53 B. Gurkan, F. Simeon and T. A. Hatton, *ACS Sustainable Chem. Eng.*, 2015, **3**, 1394–1405.

54 Chiyoda Corporation, Int. Pat., WO2023003029, 2023.

55 Y. Liu, H. Z. Ye, K. M. Diederichsen, T. Van Voorhis and T. A. Hatton, *Nat. Commun.*, 2020, **11**, 2278.

56 M. Rahimi, A. Khurram, T. A. Hatton and B. Gallant, *Chem. Soc. Rev.*, 2022, **51**, 8676–8695.

57 G. O. Larrazabal, P. Strom-Hansen, J. P. Heli, K. Zeiter, K. T. Therkildsen, I. Chorkendorff and B. Seger, *ACS Appl. Mater. Interfaces*, 2019, **11**, 41281–41288.

58 K. Xie, A. Ozden, R. K. Miao, Y. Li, D. Sinton and E. H. Sargent, *Nat. Commun.*, 2022, **13**, 3070.

59 Y. Xu, R. K. Miao, J. P. Edwards, S. Liu, C. P. O'Brien, C. M. Gabardo, M. Fan, J. E. Huang, A. Robb, E. H. Sargent and D. Sinton, *Joule*, 2022, **6**, 1333–1343.

60 IDEA Lab, LCI Database IDEA Version 3.2.0, 2023, https://idea-lca.com/en/.

61 H. H. Khoo, I. Halim and A. D. Handoko, *J. CO2 Util.*, 2020, **41**, 101229.

62 Y. C. Tan, K. B. Lee, H. Song and J. Oh, *Joule*, 2020, **4**, 1104–1120.

63 L. Xie, Y. Cai, Y. Jiang, M. Shen, J. C. Lam, J. J. Zhu and W. Zhu, *Nat. Commun.*, 2024, **15**, 10386.

64 T. Li, E. W. Lees, M. Goldman, D. A. Salvatore, D. M. Weekes and C. P. Berlinguette, *Joule*, 2019, **3**, 1487–1497.

65 J. Zhang, Y. Cao, P. Ou, G. Lee, Y. Zhao, S. Liu, E. Shirzadi, R. Dorakhan, K. Xie, C. Tian, Y. Chen, X. Li, Y. C. Xiao, A. Shayesteh Zeraati, R. K. Miao, S. Park, C. P. O'Brien, J. Ge, X. Zhou, D. Sinton and E. H. Sargent, *Nat. Commun.*, 2025, **16**, 3553.

66 A. Inoue, K. Nagita, T. Harada, S. Nakanishi and K. Kamiya, *Electrochemistry*, 2025, **93**, 117005.

67 L.-C. Weng, A. T. Bell and A. Z. Weber, *Energy Environ. Sci.*, 2019, **12**, 1950–1968.

68 L.-C. Weng, A. T. Bell and A. Z. Weber, *Energy Environ. Sci.*, 2020, **13**, 3592–3606.

69 X. He, L. Lin, X. Li, M. Zhu, Q. Zhang, S. Xie, B. Mei, F. Sun, Z. Jiang, J. Cheng and Y. Wang, *Nat. Commun.*, 2024, **15**, 9923.

70 M. R. Gerhardt, L. M. Pant, J. C. Bui, A. R. Crothers, V. M. Ehlinger, J. C. Fornaciari, J. Liu and A. Z. Weber, *J. Electrochem. Soc.*, 2021, **168**, 074503.

71 M. Jouny, W. Luc and F. Jiao, *Nat. Catal.*, 2018, **1**, 748–755.

72 J. E. Huang, F. Li, A. Ozden, A. S. Rasouli, F. P. G. D. Arquer, S. Liu, S. Zhang, M. Luo, X. Wang, Y. Lum, Y. Xu, K. Bertens, R. K. Miao, C.-T. Dinh, D. Sinton and E. H. Sargent, *Science*, 2021, **372**, 1074–1078.

73 M. Goldman, A. Prajapati, N. R. Cross, A. Clemens, A. T. Chu, L. Gutierrez, M. Marufu, E. Krall, V. Ehlinger, T. Moore, E. B. Duoss and S. E. B. Hahn, *Chem Catal.*, 2025, **7**, 101497.

74 Y. Yao, E. P. Delmo and M. Shao, *Angew. Chem., Int. Ed.*, 2025, **64**, e202415894.

75 L. D. Chen, M. Urushihara, K. Chan and J. K. Nørskov, *ACS Catal.*, 2016, **6**, 7133–7139.

76 S. Ringe, E. L. Clark, J. Resasco, A. Walton, B. Seger, A. T. Bell and K. Chan, *Energy Environ. Sci.*, 2019, **12**, 3001–3014.

77 K. Yang, X. Li, J. Guo, J. Zheng, S. Li, S. Zhang, X. Cao, T. A. Sherazi and X. Liu, *J. Membr. Sci.*, 2020, **596**, 117720.

78 H.-S. Dang and P. Jannasch, *J. Mater. Chem. A*, 2016, **4**, 17138–17153.

79 C. X. Lin, X. L. Huang, D. Guo, Q. G. Zhang, A. M. Zhu, M. L. Ye and Q. L. Liu, *J. Mater. Chem. A*, 2016, **4**, 13938–13948.

80 R. Soni, S. Miyanishi, H. Kuroki and T. Yamaguchi, *ACS Appl. Energy Mater.*, 2021, **4**, 1053–1058.

81 S. Mo, L. Du, Z. Huang, J. Chen, Y. Zhou, P. Wu, L. Meng, N. Wang, L. Xing, M. Zhao, Y. Yang, J. Tang, Y. Zou and S. Ye, *Electrochem. Energy Rev.*, 2023, **6**, 28.

82 J. Kang, W. Zheng, Y. Zhou, B. Chen, S. Chen, B. Li, C. Zhang, Z. Gong and P. Ming, *J. Power Sources*, 2025, **643**, 236991.

83 K. Ueno, H. Tokuda and M. Watanabe, *Phys. Chem. Chem. Phys.*, 2010, **12**, 1649–1658.

84 Y. Xu, J. P. Edwards, S. Liu, R. K. Miao, J. E. Huang, C. M. Gabardo, C. P. O'Brien, J. Li, E. H. Sargent and D. Sinton, *ACS Energy Lett.*, 2021, **6**, 809–815.

85 C. A. Obasanjo, G. Gao, B. N. Khiarak, T. H. Pham, J. Crane and C.-T. Dinh, *Energy Fuels*, 2023, **37**, 13601–13623.

86 P. Gyenes, A. A. Samu, D. Hursán, V. Józó, A. Serfőző, B. Endrődi and C. Janáky, *Energy Environ. Sci.*, 2025, **18**, 7124–7135.

87 B. De Mot, M. Ramdin, J. Hereijgers, T. J. H. Vlugt and T. Breugelmans, *ChemElectroChem*, 2020, **7**, 3839–3843.

88 B. Endrődi, E. Kecsenovity, A. Samu, F. Darvas, R. V. Jones, V. Török, A. Danyi and C. Janáky, *ACS Energy Lett.*, 2019, **4**, 1770–1777.